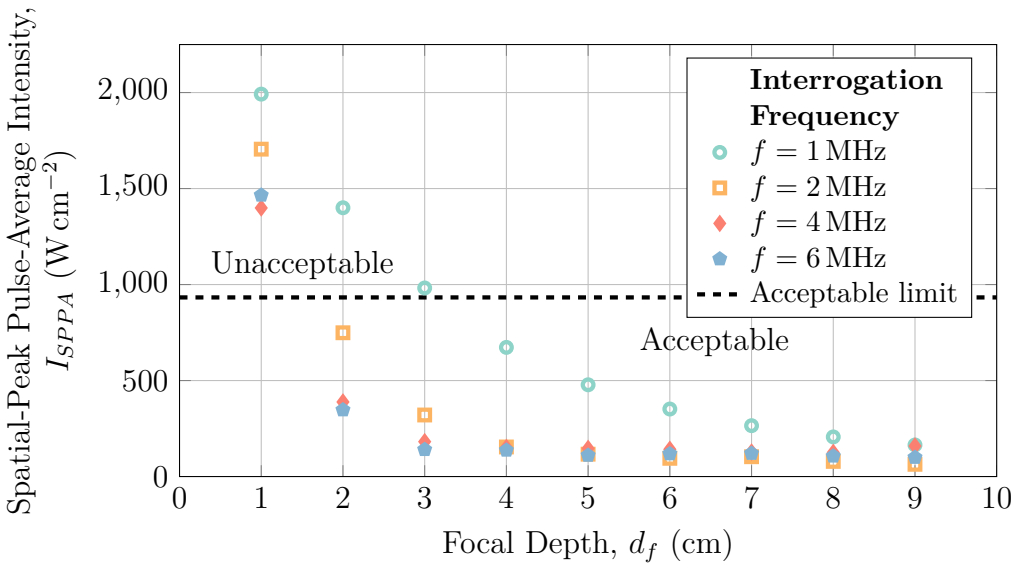

Fig. 4.8: The effect of depth and interrogation frequency on the spatial peak pulse average intensity, I_{SPPA}. I_{SPPA} is a measure of the safety of high-intensity ultrasound applications, with I_{SPPA} values below 933 W cm^{-2} considered acceptable for non-cardiovascular and non-fetal imaging.

4.3.2 Temporal Finite-Element Model of Soft Tissue Deformation

As ARFI imaging relies upon the detection of soft tissue deformation in response to the transducer-applied acoustic radiation force, a key parameter of interest is the magnitude of the deformation generated in the tissue in response to the applied loads. To this end, the temporal finite-element model of soft tissue deformation described in Section 4.2.3 was used to determine the magnitude of the deformation caused by varying acoustic radiation force parameters.

Fig. 4.9 show the relationship between the maximum induced tissue displacement, $|v|_{max}$, generated by acoustic radiation forces in soft tissue for a range of focal depths and interrogation frequencies. As expected, significantly

greater deformation is generated with shallower focal depths. Further, increases in the interrogation frequency generally resulted in lesser displacement induced in the tissue. The results obtained using a 1 MHz interrogation frequency stood apart from the higher frequencies investigated. This is likely due to the excess acoustic radiation force produced at such low frequencies shown in Figs. 4.4 and 4.8.

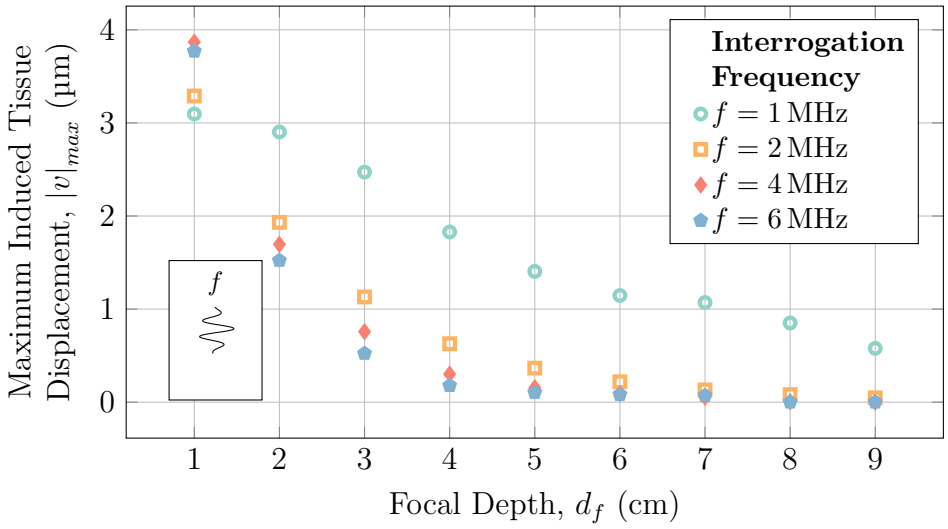

Fig. 4.9: Magnitude of deformation resulting from ARFI interrogation at various focal depths and interrogation frequencies with a transducer aperture of 4 cm and source pressure of 3.35 MPa.

To reiterate the results seen in Fig. 4.7, the maximum induced tissue displacement generated by the applied acoustic radiation force at various focal depths for various source pressures was investigated, the results of which are given in Fig. 4.10. These results echo the results seen in Fig. 4.7, where doubling the applied pressure resulted in approximately quadrupling the maximum displacement seen in the tissue across all focal depths as was expected.

The results given in Fig. 4.10 were further investigated by examining the effect of the interrogation frequency on the maximum induced tissue dis-

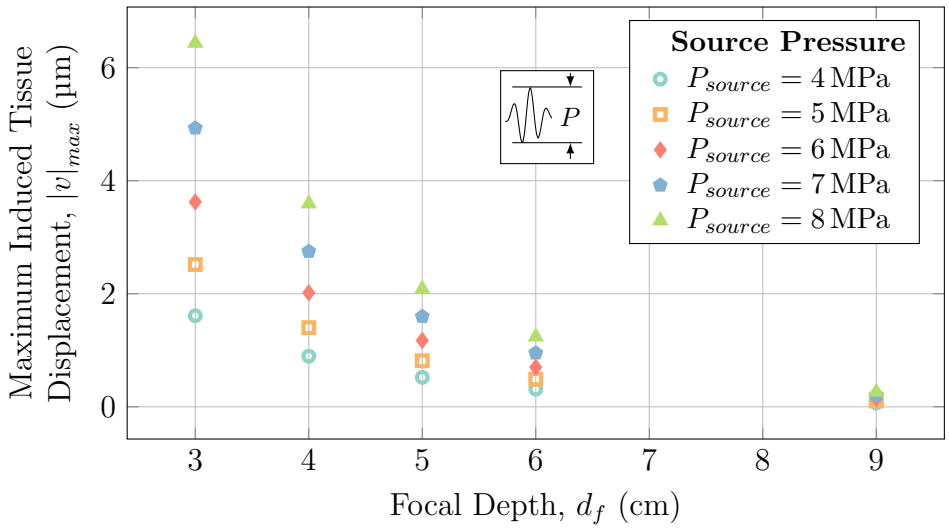

Fig. 4.10: Magnitude of deformation resulting from ARFI interrogation at various focal depths and source pressures at an interrogation frequency of 2 MHz with a transducer aperture of 4 cm and source pressure of 3.35 MPa.

placement. As expected, increasing the interrogation frequency resulted in decreases in the magnitude of deformation experienced by the tissue across all source pressures investigated. Further, increasing the amount of source pressure applied by the transducer into the tissue resulted in greater levels of tissue deformation. Of note is that the use of a 1 MHz interrogation frequency affected the magnitude of tissue deformation across the different source pressures much more than any of the higher interrogation frequencies studied, further echoing the results seen in Fig. 4.9.

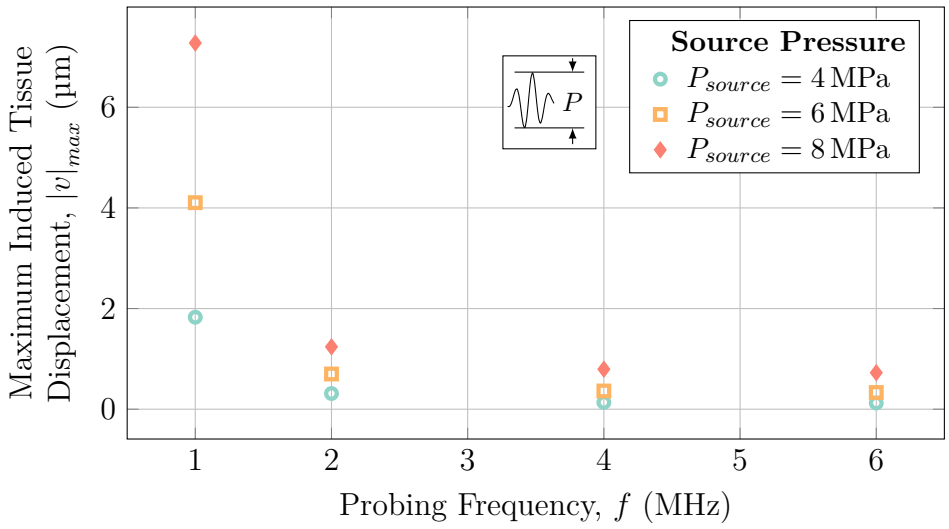

Fig. 4.11: Magnitude of deformation resulting from ARFI interrogation at various interrogation frequencies and source pressures at a depth of 6 cm with a transducer aperture of 4 cm and source pressure of 3.35 MPa.

4.3.3 Numerical Characterization of Acoustic Radiation Force Impulse Imaging

Beyond understanding the general nature of acoustic radiation forces in soft tissue, the effects of these forces in the presence of deep tissue injuries must also be characterized for ARFI imaging to become a useful diagnostic tool for such injuries. In order to investigate the suitability of ARFI imaging for the detection of DTI, the procedure outlined in Section 4.2.4 was carried out on a range of models with varying parameters of interest. The results of these characterizations are presented here.

In order to understand the effect of general lesion size on the detection sensitivity of ARFI imaging, hard-boundaried spherical lesions of various radii were placed in a soft tissue domain at a depth of 4 cm and insonated at 2 MHz with an aperture of 4 cm and pressure of 3.35 MPa for 150 µs (300 pulse cycles). The results of this characterization are presented in Fig. 4.12.

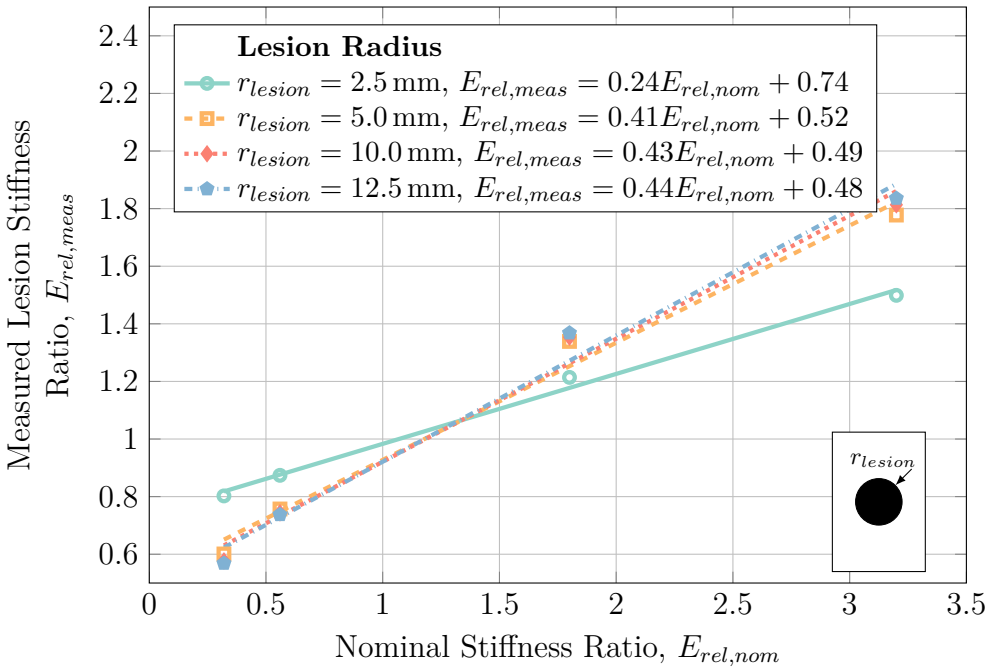

Fig. 4.12: Numerical characterization of the ARFI imaging-acquired stiffness ratios acquired with varying lesion radii for a hard-boundaried lesion at a depth of 4 cm using an ARFI probing frequency of 2 MHz.

As Fig. 4.12 shows, ARFI imaging was able to detect the presence of both stiff and unstiff lesions of all sizes, however the technique both severely underestimated the stiffness of stiff lesions and overestimated the stiffness of unstiff lesions—leading to the observation that ARFI imaging has a relatively low detection sensitivity with regards to both stiff and unstiff deep tissue injury lesions. Fig. 4.12 also shows that above lesion radii of approximately 2.5 mm, the lesions size does not have any appreciable effect on the detection sensitivity of the technique. Below this limit, however, lesions will be much more difficult to detect as the differences between them and the surrounding tissue are minimized.

To further corroborate these results, the mean-squared error associated with the various lesion radii was calculated according to equation 4.17 where

$\hat{Y}_i$ are the true lesion stiffness ratios and Y_i are the measured lesion stiffness ratios. The results of this calculation with regards to lesion radius are given in Fig. 4.13. Figure 4.13 explicitly depicts a greater degree of error for lesions with radii of 2.5 mm, with only marginal improvements in measurement error resulting from increasing the lesion radius beyond 5.0 mm.

$$MSE = \frac{1}{n}\sum_{i=1}^{n}\left(\hat{Y}_i - Y_i\right)^2 \tag{4.17}$$

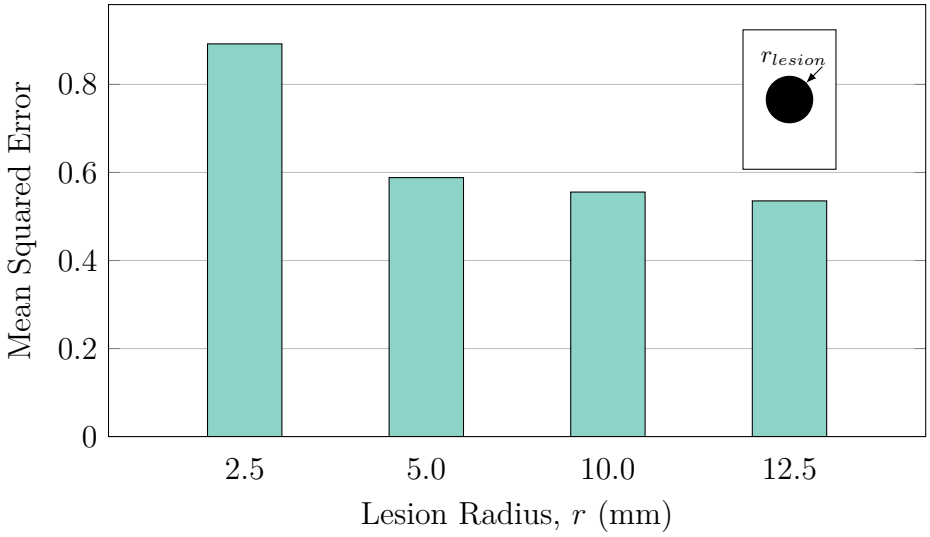

Fig. 4.13: Mean squared error between the true and measured lesion stiffness ratios for increasing lesion radii for a hard-boundaried lesion at a depth of 4 cm using an ARFI interrogation frequency of 2 MHz.

In order to investigate the effect of lesion depth on detection sensitivity, the use of ARFI imaging to distinguish spherical hard-boundaried lesions with radii of 10 mm was investigated at a range of depths, with the results shown in Fig. 4.14. As Fig. 4.14 shows, there is almost no dependence of the detection sensitivity on the depth of the lesion. However, it must be noted that the deformations resulting from acoustic radiation force impulses will be of such small magnitudes that they will not be detectable using current ultrasound

technology. To understand the limitations of depth in ARFI imaging, please refer to Section 4.3.2.

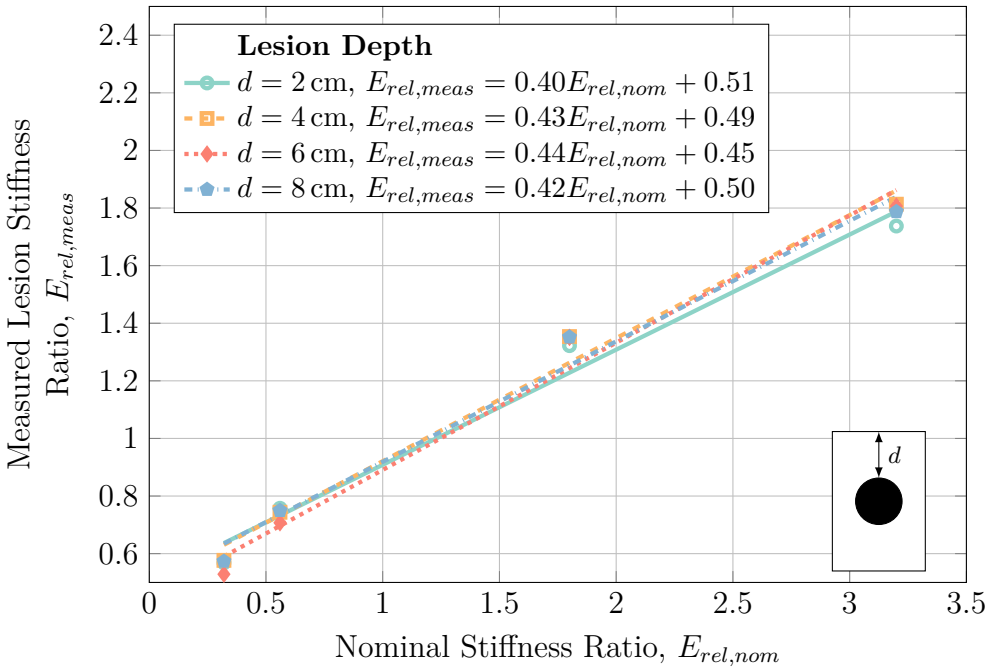

Fig. 4.14: Numerical characterization of the ARFI imaging-acquired stiffness ratios acquired with varying lesion and focal point depths for a hard-boundaried 0.5 cm radius lesion using an ARFI probing frequency of 2 MHz.

Fig. 4.15 portrays the mean-squared-error of the measured lesion stiffness across the various depths examined. Although the variance in error between the different depths is not substantial, both very shallow—lesions at a depth of 2 cm or less—and very deep—lesions at a depth of 8 cm or more—were found to have the greatest measurement error. In shallow tissue, this increase in error may be due to an inability to appropriately focus the acoustic radiation force so close to the transducer whereas in deep tissue, the increase in error is likely due to the reduced magnitude of radiation force present due to the relatively large amount of tissue absorption.

Since the aforementioned hard-boundaried, spherical lesion cases represent

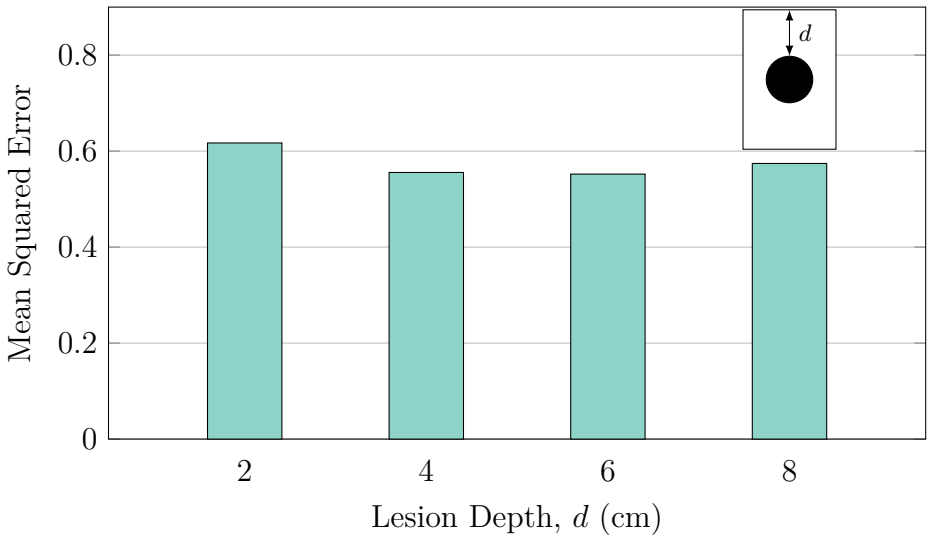

Fig. 4.15: Mean squared error between the true and measured lesion stiffness ratios for increasing lesion depths for a hard-boundaried 0.5 cm radius lesion using an ARFI interrogation frequency of 2 MHz.

simplifications of reality designed to obtain a general understanding of the ARFI technique, models representing more complicated geometry were also studied. Fig. 4.16 shows the simulated lesion stiffness ratios for a set of lesions with radii of 10 mm at a depth of 4 cm with blurred boundaries as described in Section 4.2.4. As Fig. 4.16 shows, there is no reliance of the detection sensitivity on the blur radius of the lesion, with the results shown repeating the results seen in Figs. 4.12 and 4.14.

The mean-squared error shown in Fig. 4.17 further supports this conclusion, with the error between different blur radii differing by just over 1 %. This lack of sensitivity on the degree of lesion blurring presents a significant advantage over quasi-static elastography as it allows even lesions without well-defined boundaries to be detected.

It may also be possible that a diseased region of tissue is not a singular, continuous lesionous region, but rather an amalgamation of numerous small

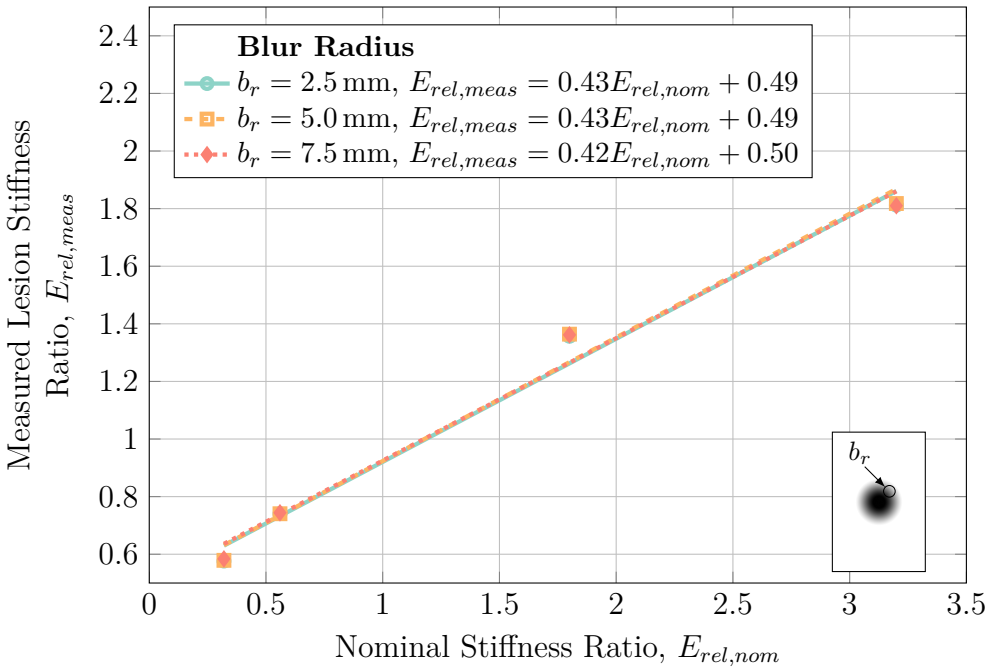

Fig. 4.16: Numerical characterization of the ARFI imaging-acquired stiffness ratios acquired with varying lesion and focal point depths for a blurred 1.0 cm radius lesion at a depth of 4 cm using an ARFI interrogation frequency of 2 MHz.

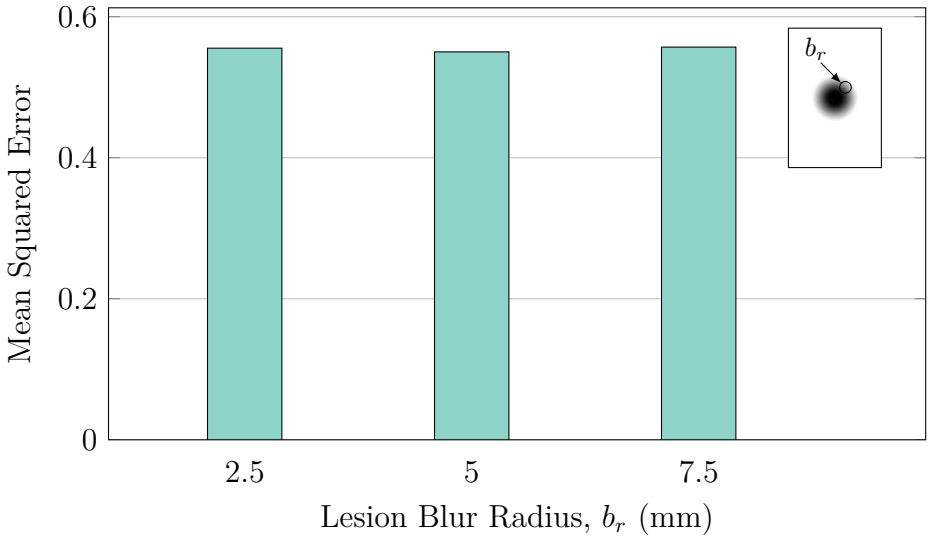

Fig. 4.17: Mean squared error between the true and measured lesion stiffness ratios for increasing lesion depths for a blurred 1.0 cm radius lesion at a depth of 4 cm using an ARFI interrogation frequency of 2 MHz.

lesions or damaged tissue which collectively compose a larger lesionous region. To investigate the effect such a phenomenon would have on the detection sensitivity of ARFI imaging, the density and size of numerous small, clustered lesions were varied in models and the resulting measured stiffness ratios were investigated. Fig. 4.18 shows the characterization of the lesion cluster density—how many lesions are present per unit area—for densities ranging from $10\,\mathrm{cm}^{-2}$ to $40\,\mathrm{cm}^{-2}$ with small lesions of radius 1.0 mm. The centre of the lesionous regions were located at a depth of 4 cm in an overall region with a radius of 10 mm.

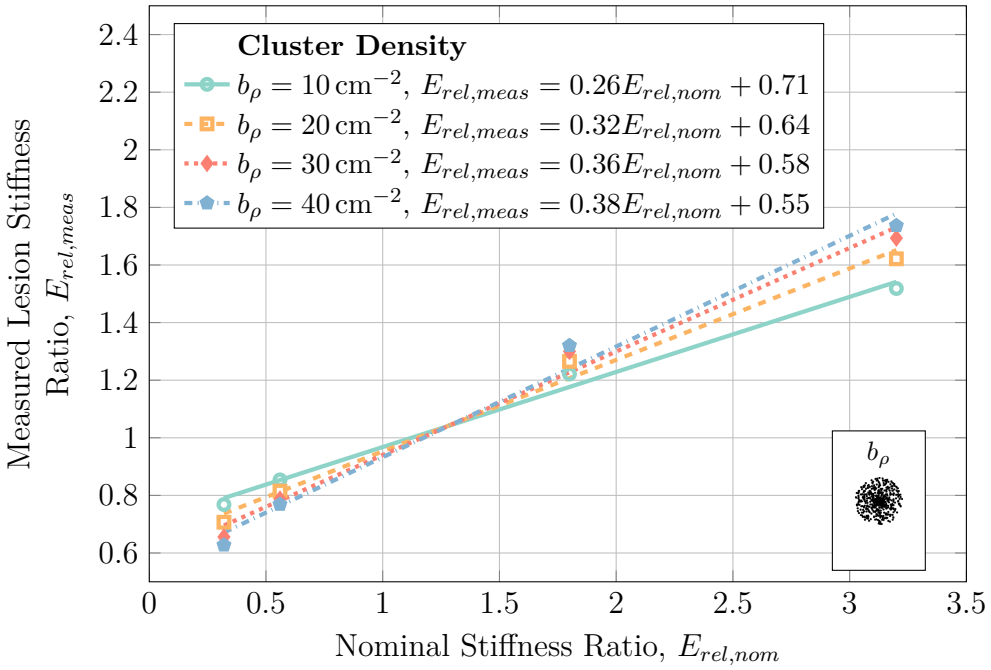

Fig. 4.18: Numerical characterization of the ARFI imaging-acquired stiffness ratios acquired with varying cluster densities for clustered 1 mm radius lesions within a 1.0 cm radius at a depth of 4 cm using an ARFI interrogation frequency of 2 MHz.

As Fig. 4.18 shows, increasing the cluster density results in monotonically increasing the detection sensitivity of the ARFI technique. This is as expected, as increasing the cluster density increases the total area contributing to the

modified tissue stiffness in the region, which in turn allows the ARFI technique to more readily distinguish the lesion. These results are further shown by the mean-squared error shown in Fig. 4.19 which shows the decrease in error attributed to increases in lesion cluster densities.

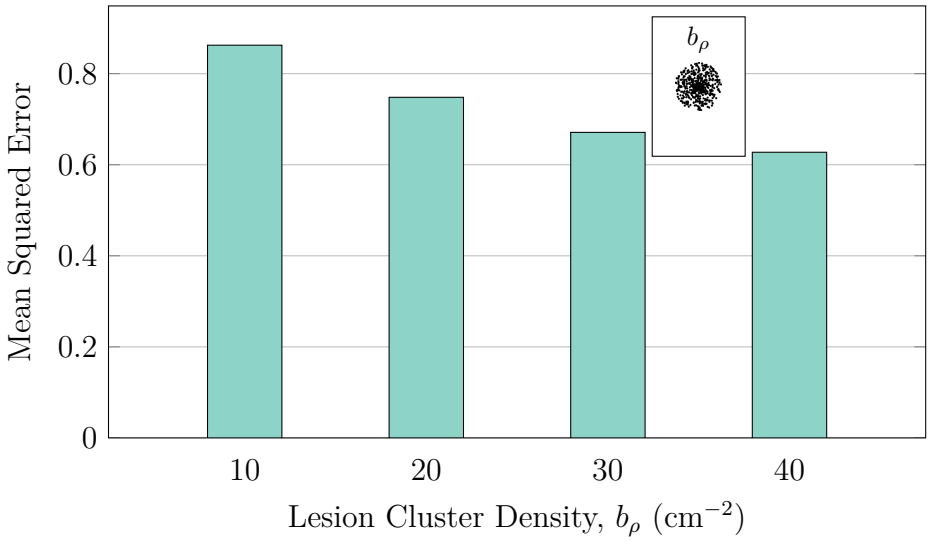

Fig. 4.19: Mean squared error between the true and measured lesion stiffness ratios for increasing lesion cluster density for clustered 1 mm radius lesions within a 1.0 cm radius at a depth of 4 cm using an ARFI interrogation frequency of 2 MHz.

Another method to alter the ratio of damaged to healthy tissue within the lesionous region is to alter the size of the individual lesions that comprise that region. This characterization was carried out using small lesions with radii ranging from 0.5 mm to 1.5 mm at a cluster density of 30 cm^{-2}, with the results given in Fig. 4.20.

As Fig, 4.20 shows, decreasing the individual lesion radii in the clustered model substantially decreased the detection sensitivity of the ARFI technique, again echoing the previous results where decreasing the ratio of damaged to healthy tissue in the lesionous region results in lesser detection sensitivity. This is confirmed by examining the mean-squared error of the results, which

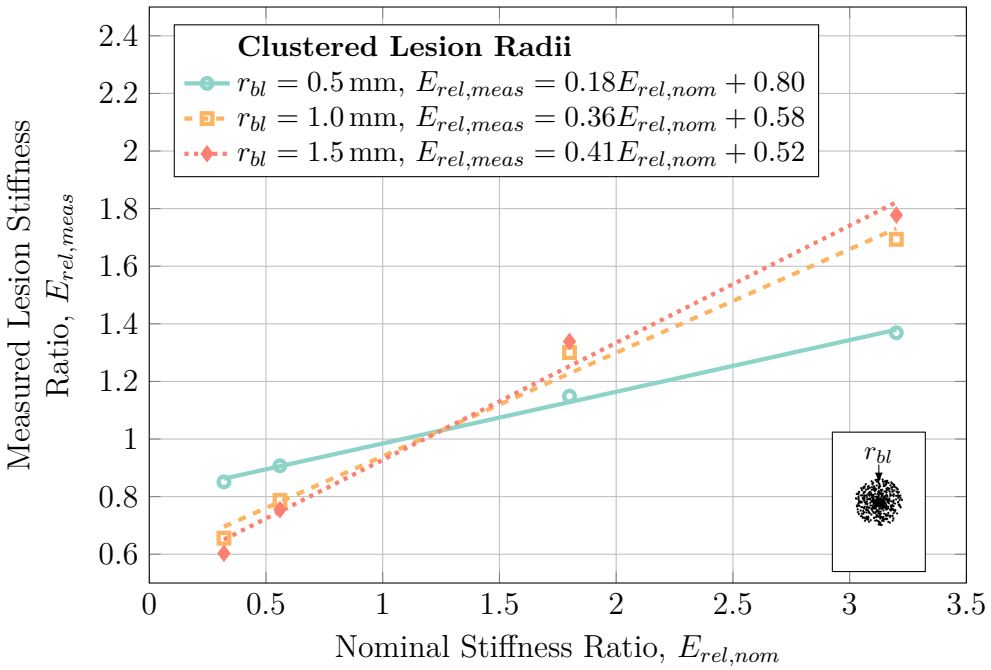

Fig. 4.20: Numerical characterization of the ARFI imaging-acquired stiffness ratios acquired with varying clustered lesion radii for clustered lesions with a density of $30\,\text{cm}^{-2}$ within a 1.0 cm radius at a depth of 4 cm using an ARFI interrogation frequency of 2 MHz.

shows monotonically decreasing errors for monotonically increasing individual lesion radii.

While the aforementioned studies investigated generally spherical lesionous regions, this is unlikely to be the case in a real soft tissue domain. To further investigate ARFI imaging, a model utilizing complicated geometry arising from the combination of the MRI-acquired geometry of a deep tissue injury with the anatomical distribution of fat, muscle, and bone obtained from the Visible Human project [126] was created as described in Section 4.2.4. To investigate the effect of lesion size in this model, the lesion size, $\varnothing L$, was varied between 2.5 mm and 12.5 with the lesion being placed at a depth of 6 cm. The results of this characterization are shown in Fig. 4.22.

As Fig. 4.22 shows, decreasing the lesion width in the Visible Human

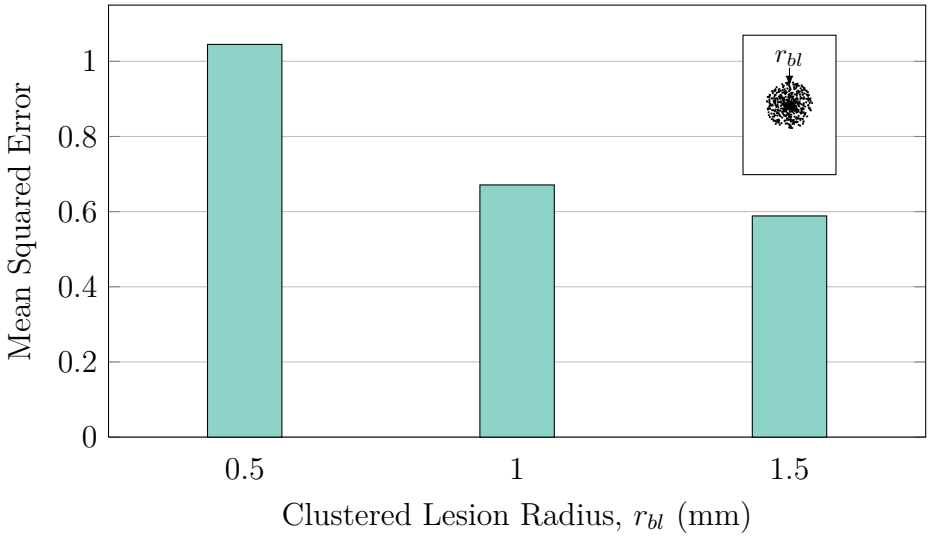

Fig. 4.21: Mean squared error between the true and measured lesion stiffness ratios for increasing clustered lesion radii for clustered lesions with a density of $30\,\mathrm{cm}^{-2}$ within a 1.0 cm radius at a depth of 4 cm using an ARFI interrogation frequency of 2 MHz.

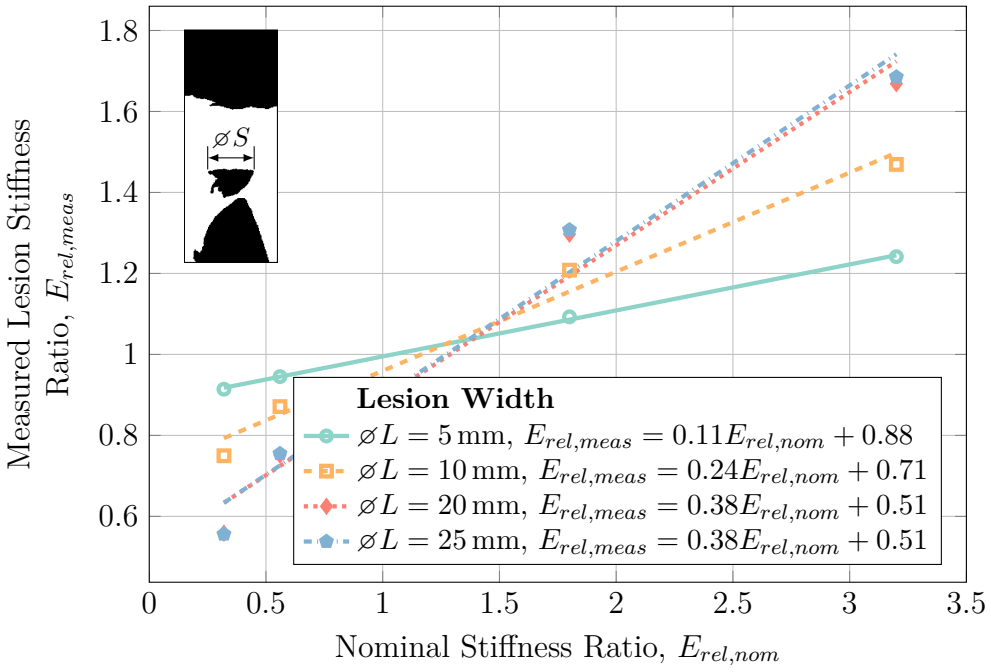

Fig. 4.22: Numerical characterization of ARFI imaging-acquired stiffness ratio with changing lesion radii for MRI-acquired lesion geometry in a Visible Human model at a depth of 6 cm using an ARFI interrogation frequency of 2 MHz.

model resulted in a decreased detection sensitivity which was echoed by the mean-square error of the results shown in Fig. 4.23. The detection sensitivity decreases with half-widths less than 10 mm in the Visible Human model as opposed to radii of 5 mm as found with the spherical lesion embedded in general soft tissue seen in Fig. 4.12. Although the reason for this is not immediately clear, possible differences lay in the depth at which the lesions were imaged at: the Visible Human model placed the lesion at a depth of 6 cm so as to have it lay immediately superior to the ischial tuberosity while the results for the spherical lesion were taken at a depth of 4 cm. Further, comparing the half-width of the Visible Human lesion to the radius of the spherical lesion may introduce errors as the overall area of lesionous tissue were different.

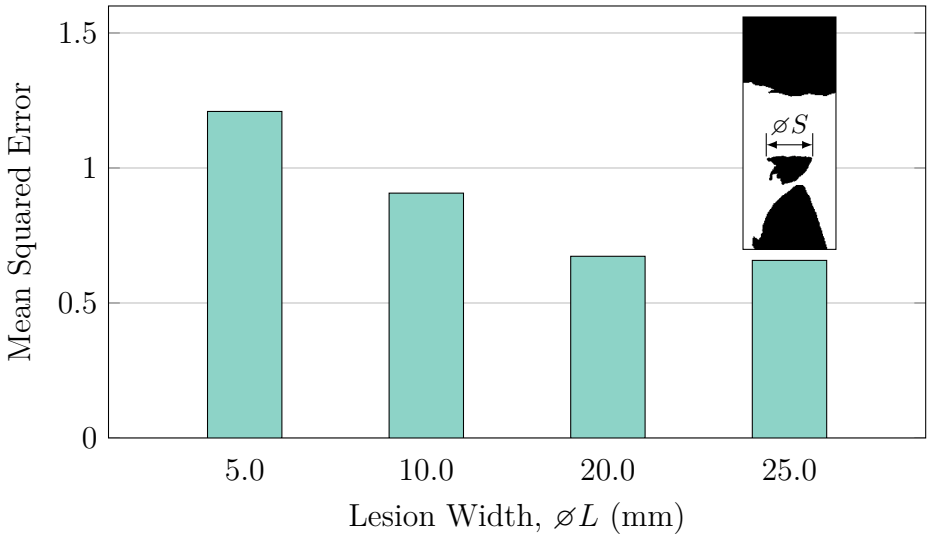

Fig. 4.23: Mean squared error between the true and measured lesion stiffness ratios for increasing lesion radii for MRI-acquired lesion geometry in a Visible Human model at a depth of 6 cm using an ARFI interrogation frequency of 2 MHz.

Numerical values for the characterization plots presented here are given in Section A.2 of Appendix A.

4.3.4 Physical Phantom Validation

In order to determine if the results presented in Section 4.3.3 represent valid simulations, validation experiments were carried out on a physical tissue mimicking phantom as described in Section 4.2.5. Fig. 4.24 shows the result of these experiments.

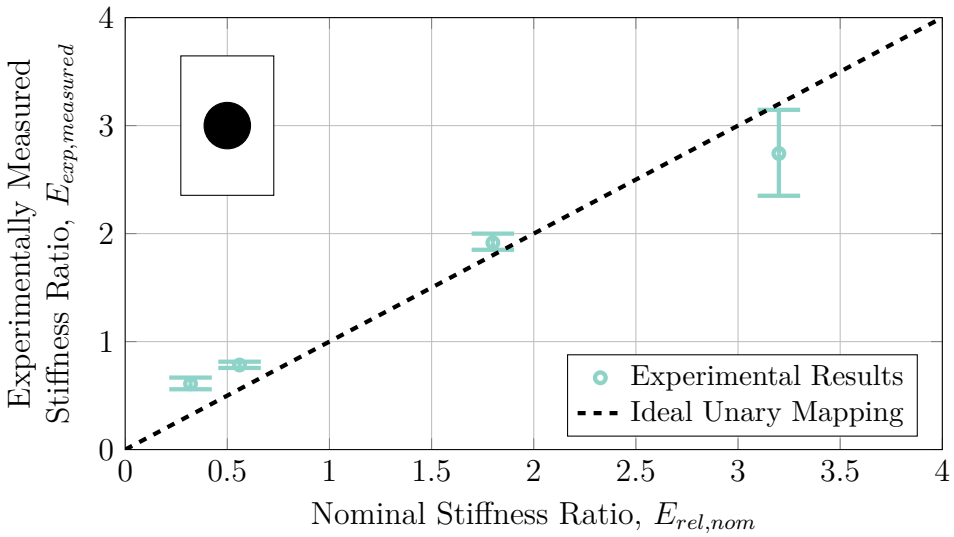

Fig. 4.24: Relation between nominally reported strain ratios of the tissue mimicking phantom and experimentally measured strain ratios for a lesion at a depth of 3.5 cm and diameter of 2.0 cm. Error bars represent the range of measurements acquired.

As the results seen in Fig. 4.24 show, ARFI imaging was found experimentally to significantly underestimate the stiffness of the stiffest lesions investigated—lesions with nominal stiffnesses of 3.2. For all other lesions investigated, ARFI imaging was shown to overestimate the lesion stiffness slightly. Although it is possible that the true stiffness ratio of the lesions in the phantom do not perfectly align with the manufacturer-reported nominal values, it is also possible that the acoustic radiation force developed by the ARFI transducer was not enough to substantially deform the stiffest of lesions, leading to

the stiffness being underestimated.

Fig. 4.25 compares the experimentally-acquired lesion stiffness ratios against measured stiffness ratios arising from parametrically identical simulated lesions. As Fig. 4.25 shows, although the experimentally measured stiffness ratios align well with the simulated stiffness ratios for relatively unstiff lesions ($E_{rel} < 1$), the simulated ARFI procedure was found to underestimate the stiffness of the stiff lesions that were investigated ($E_{rel} > 1$). The exact cause of this disparity is unclear and future work must be done in order to remedy this in the simulations that were performed in order to accurately understand ARFI imaging.

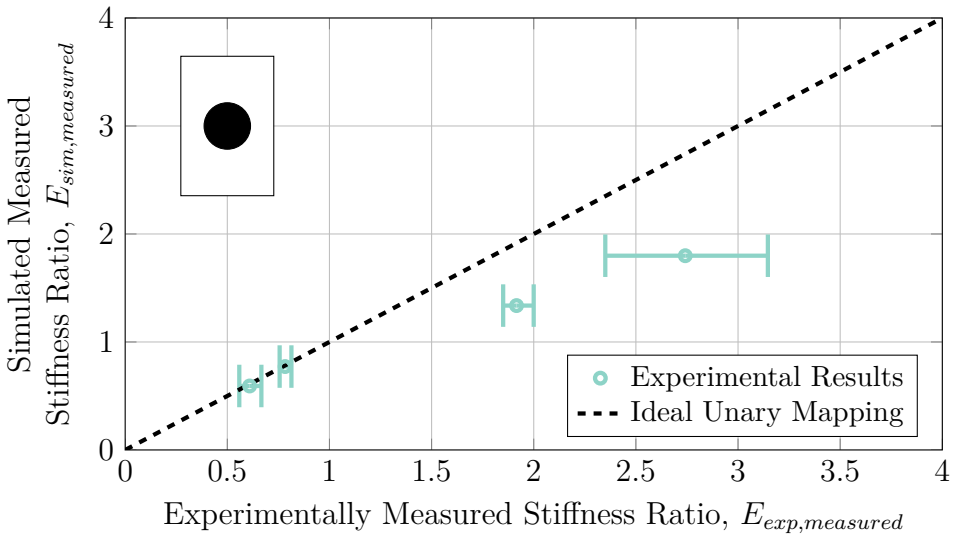

Fig. 4.25: Relation between simulated measured strain ratios and experimental measured strain ratios for a lesion at a depth of 3.5 cm and diameter of 2.0 cm.

4.4 Conclusion

The results presented in Section 4.3 represent a numerical characterization of the use of acoustic radiation force impulse imaging for the detection of deep